Influence of the Adjacency Effect on Ground Reflectance Measurements

Rudolf Richter, Martin Bachmann, Wouter Dorigo, and Andreas Müller

***Abstract*—It is well known that the adjacency effect has to be taken into account during the retrieval of surface reflectance from high spatial resolution satellite imagery. The effect results from atmospheric scattering, depends on the reflectance contrast between a target pixel and its large-scale neighborhood, and decreases with wavelength. Recently, ground reflectance field measurements were published, claiming a substantial influence of the adjacency effect at short distance measurements (< 2 m), and an increase of the effect with wavelength. The authors repeated similar field measurements and found that the adjacency effect usually has a negligible influence at short distances, decreasing with wavelength in agreement with theory, but can have a small influence in high-reflectance contrast environments. Radiative transfer calculations were performed to quantify the influence at short and long distances for cases of practical interest (vegetation and soil in a low-reflectance background). For situations with large reflectance contrasts, the atmospheric backscatter component of the adjacency effect can influence ground measurements over small-area targets, and should therefore be taken into account. However, it is not possible to draw a general conclusion, since some of the considered surfaces are known for exhibiting strong directional effects.**

***Index Terms*—Adjacency effect, atmospheric scattering, ground measurements, surface reflectance.**

I. Introduction

THE ADJACENCY effect is an interesting physical phenomenon caused by atmospheric crosstalk between fields of different surface reflectance (see Fig. 1). Radiation component 1 represents path radiance, i.e., photons without ground contact scattered in the air volume between ground and sensor, and component 2 is the global (direct plus diffuse) solar radiation reflected from the target and transmitted to the sensor. Components 3 and 4 represent the adjacency effect, i.e., reflected background radiation scattered into the instantaneous field of view (FOV) and radiation backscattered to the ground by the atmosphere [spherical albedo parameter; see (1) and (2)]. The last two components are often combined into a single adjacency component compliant with the third term of (3). Only the signal component 2 contains information on the target surface reflectance ρ_{t} to be retrieved with atmospheric correction; the other components have to be calculated and removed from the total signal.

The motivation for this letter is a check of measurements published in [1] where a substantial influence of the adjacency effect was claimed for short-range ground measurements, increasing with wavelength. Since this can hardly be explained by a physical model our contribution evaluates similar measurements and includes a theoretical radiative transfer analysis.

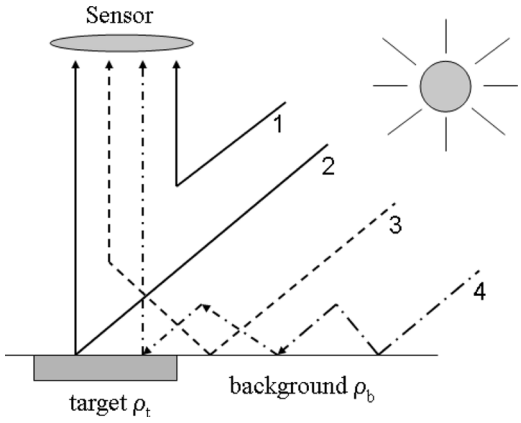

Fig. 1. Schematic sketch of radiation components (see text for a detailed explanation).

The adjacency effect has been studied since 1977 [2]–[7] and can be observed in high spatial resolution (< 100 m) imagery, especially in the 400–1000-nm region. Its influence decreases with wavelength because atmospheric scattering efficiency decreases.

The radiation transfer for a large homogeneous Lambertian surface of ground reflectance ρ is described by [6], [7]

$$L_{\mathrm{total}}(\rho) = L_p + \frac{\tau E_g(0)\rho/\pi}{1 - s\rho} = L_p + \tau E_g(\rho)\rho/\pi \qquad (1)$$

where L_{total}, L_p, τ, $E_g(0)$, and s are the total at-sensor radiance, path radiance, total ground-to-sensor transmittance, global flux on the ground for $\rho = 0$, and the spherical albedo of the atmosphere, respectively. The total transmittance τ is the sum of the direct and diffuse transmittances, i.e., $\tau = \tau_{\mathrm{dir}} + \tau_{\mathrm{dif}}$. Equation (1) shows that the effective global flux $E_g(\rho) = E_g(0)/(1 - s\rho)$ depends on the ground reflectance and spherical albedo. For a small target of reflectance ρ_{t} in a large background of reflectance ρ_{b}, the at-sensor radiance can be calculated as [7]

$$L_{\mathrm{total}}(\rho) = L_p + \frac{\tau_{\mathrm{dir}} E_g(0)\rho_{\mathrm{t}}/\pi}{1 - s\rho_{\mathrm{b}}} + \frac{\tau_{\mathrm{dif}} E_g(0)\rho_{\mathrm{b}}/\pi}{1 - s\rho_{\mathrm{b}}}. \qquad (2)$$

In our presentation, it is more convenient to reformulate (2) as

$$L_{\mathrm{total}}(\rho) = L_p + \frac{\tau E_g(0)\rho_{\mathrm{t}}/\pi}{1 - s\rho_{\mathrm{b}}} + \frac{\tau_{\mathrm{dif}} E_g(0)(\rho_{\mathrm{b}} - \rho_{\mathrm{t}})/\pi}{1 - s\rho_{\mathrm{b}}} \qquad (3)$$

Manuscript received April 17, 2006; revised June 2, 2006.

The authors are with German Aerospace Center (DLR), Remote Sensing Data Center, 82234 Wessling, Germany (e-mail: rudolf.richter@dlr.de).

Digital Object Identifier 10.1109/LGRS.2006.882146

which emphasizes the fact that the adjacency component 3, i.e., the last term of (3), is directly proportional to the target/background reflectance contrast.

The horizontal range of the adjacency effect is typically 1–2 km for satellite imagery which is the same magnitude as the boundary aerosol scale height [7]. For very clear atmospheric conditions (low aerosol concentration), the molecular (Rayleigh) scattering dominates in the 400–700-nm region, and a larger adjacency range up to 6–10 km can be expected, in agreement with the Rayleigh scale height of 6.3 km [6]. Efficient approximations have been developed to account for the adjacency effect during the atmospheric correction of satellite imagery [8], [9].

Since the adjacency effect is caused by Rayleigh and aerosol scattering, it depends on the air volume between the target and the measuring device, i.e., a large volume and a high optical thickness increase the scattering probability (components 3 and 4 of Fig. 1). Therefore, the effect should be very small for short-distance measurements (< 2 m) between spectrometer and target which are typically used for inflight calibration experiments [10]–[12]. Only radiation component 4 of Fig. 1 (atmospheric backscattering) can exert an influence in this case because the background reflectance ρ_{b} (if different from ρ_{t}) modifies the global flux on the ground. Since field measurements during inflight calibrations are conducted during clear weather conditions, this influence factor should be small, and it is quantified in this letter. However, a recent publication [1] claims a large influence of the adjacency effect for ground measurements and an increase with wavelength. Such physical characteristics are hardly possible as the scattering efficiency of aerosols and molecules decreases with wavelength. This contribution repeated field measurements similar to those conducted by the authors of [1], and we were not able to support their findings and conclusions.

II. Ground Measurements

Atmospheric and ground measurements are often performed for calibration/validation of satellite instruments. They require accurately calibrated ground instrumentation and large homogeneous fields compared to the spatial resolution of the satellite instrument. A detailed discussion of the critical points for these measurements can be found in [10]–[12]. A wide FOV spectroradiometer is often used to facilitate a proper spatial sampling of the fields [13], and it was also employed in our case.

On April 7, 2006, field measurements were conducted on the German Aerospace Center (DLR) campus in Wessling about 25 km west of Munich employing two targets (bare soil and a dense garden cress vegetation canopy) that were recorded in two types of large background fields (concrete and meadow) to study the neighborhood effect.

The measurements were performed with an Analytical Spectral Devices (ASD) FieldSpec Pro instrument [14] using a 25° FOV at a distance $h_2 = 22$ cm for two cases (see Fig. 2) (target at the ground $h_1 = 0$, and elevated on a tripod at height $h_1 = 1.5$ m, cases (a) and (b), respectively, nadir view). The 25° wide FOV mode of the ASD was used because it enables a larger footprint, i.e., a better spatial sampling of the target. This setup was probably also employed in [1], although a detailed description is missing there (Fig. 1 of [1] suggests a measurement distance of 1.5 m for case (a), and Fig. 2 suggests a 20-cm distance as mentioned in the text "*The detector was operated at 0.2 m height in the nadir direction*"). The drawback of the wide FOV mode is a somewhat larger sensitivity to bidirectional effects as documented in [15]. We included the elevated target case for comparison with [1], although this setup is based on the erraneous assumption that multiple scattering only occurs below an instrument, whereas the radiation components 3 and 4 of Fig. 1 still contribute for an elevated target.

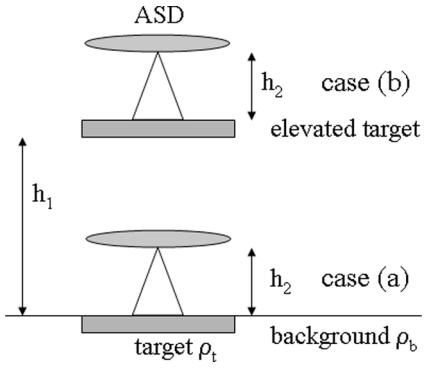

Fig. 2. Geometric setup for ground reflectance measurements ($h_1 = 1.5$ m, $h_2 = 22$ cm).

With $h_2 = 22$ cm, the ASD footprint is 9.6 cm in diameter. The target and a white Spectralon reference panel were measured alternately. For each target ten single measurements were taken and averaged, and for the two background fields 20–30 measurements from different locations were averaged. Both targets were also measured in the laboratory using a 1000-W halogen light source, about 2 h before the field campaign. The geometric setup in the lab was the same as for the field measurements, the sole difference being the halogen source (instead of the sun) which was placed 0.5 m above the target at a zenith angle of 30°. The illumination footprint was narrowly concentrated on the target that was placed on a large black cloth. A very small fraction of the light cone met the black cloth and was mainly absorbed, thus minimizing any influence of reflected stray light. The lab setup inherently lacks the hemispherical diffuse illumination present at field measurements which is critical for vegetation canopies [15]. Therefore, compared to the soil case, somewhat larger differences between lab and field measurements can be expected for the garden cress (compare Figs. 3–6). All measurements were corrected for detector drift and the Spectralon reflectance characteristics.

Figs. 3–6 show the results. The solid, dotted, and dashed curves represent the laboratory measurement and field measurement with the target at ground (case a), and target at 1.5-m elevation (case b), respectively. It can be seen that the reflectance spectra are almost the same for the soil target at ground level and for the elevated target (Figs. 3 and 4). This can be expected, because the volume of the air layer between target and ASD is the same for both setups, and the small vertical displacement does not alter the optical properties of the air. Therefore, both adjacency radiation components

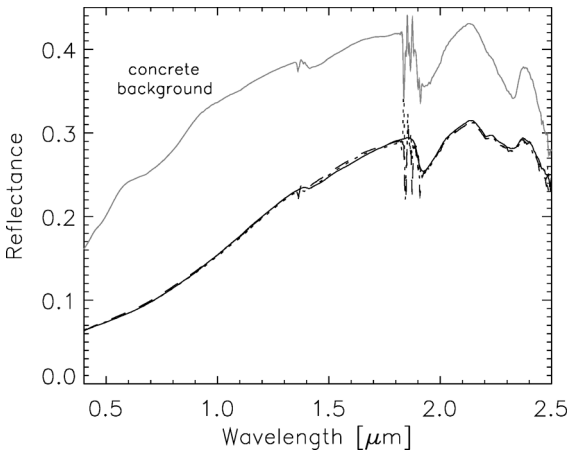

Fig. 3. Soil in concrete background. The solid, dotted, and dashed curves represent measurements in the laboratory and those for cases (a) and (b), respectively.

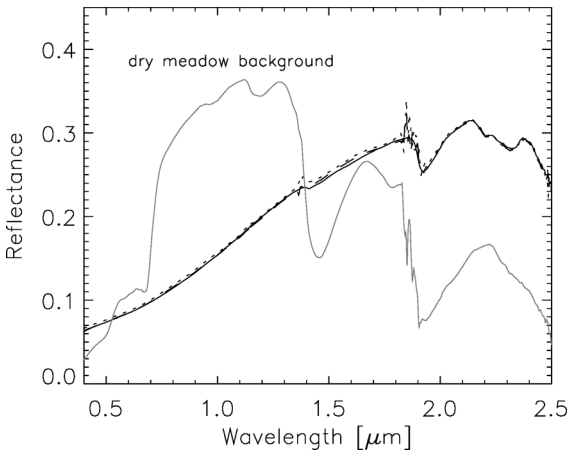

Fig. 4. Soil in dry meadow background. The solid, dotted, and dashed curves represent measurements in the laboratory and those for cases (a) and (b), respectively.

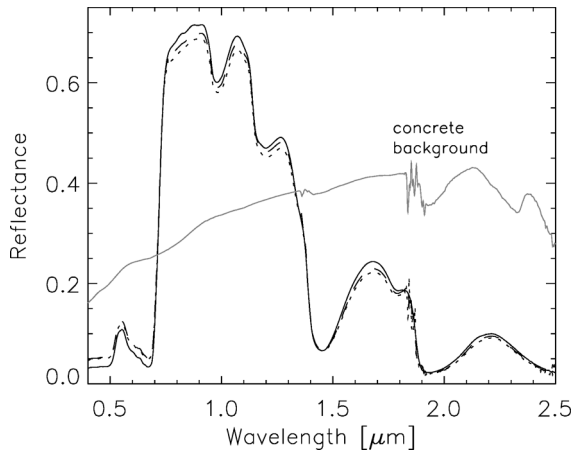

Fig. 5. Garden cress in concrete background. The solid, dotted, and dashed curves represent measurements in the laboratory and those for cases (a) and (b), respectively.

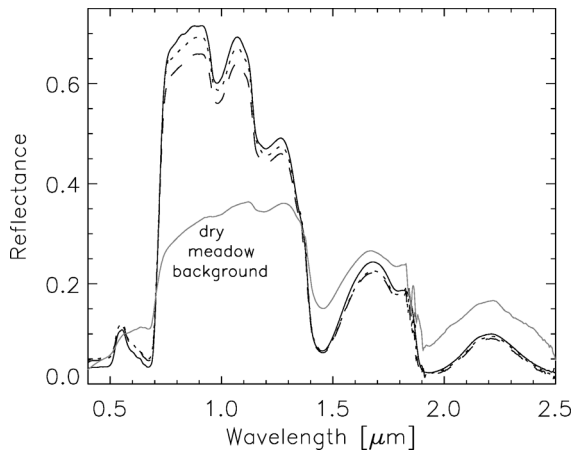

Fig. 6. Garden cress in dry meadow background. The solid, dotted, and dashed curves represent measurements in the laboratory and those for cases (a) and (b), respectively.

(3 and 4 of Fig. 1) do not change when altering the setup. The field measurements almost coincide with the laboratory spectrum because the soil target is very homogeneous. This close agreement also holds in the 2–2.5-μm region, indicating that the influence of the adjacency effect is very small there contrary to results of [1]. The noisy appearance of the field spectra in the 1.8-μm region is caused by strong atmospheric water vapor absorption, i.e., a very low solar illumination.

Results for the garden cress (Figs. 5 and 6) cannot be interpreted as easily because the standard deviation of the reflectance is larger than for the soil target. For example, Fig. 5 shows a difference of 0.01 units at 0.9 μm between cases (a) and (b), while Fig. 6 shows a difference of 0.02 units although the target-background reflectance contrast is about the same. In addition, in case (a) the reflectance level of the cress (at 0.9 μm) changes from 0.69 (concrete background) to 0.64 (dry meadow background). As mentioned above, these somewhat larger differences between lab and field measurements can be expected, because of the bidirectional reflectance behavior of vegetation canopies and because laboratory measurements inherently lack the diffuse hemispherical illumination [15]. In addition, there was a 5° change in the solar zenith angle during the 1-h field campaign. The difference is still within the two standard deviation margin of the field measurements, i.e., a 95% probability confidence interval also includes the laboratory curve. These results demonstrate that differences in the 1.6- and 2.2-μm region at large reflectance contrasts (0.20 to 0.35 units) are very small for all situations contrary to the measurements of [1]. Our experimental results are also in agreement with radiative transfer calculations presented next.

III. Radiative Transfer Calculations

As an accurate theoretical analysis of the radiative transfer in the Earth's atmosphere cannot be performed with a simple analytical model some numerical calculations with the established MODTRAN code [16] are conducted to investigate the potential influence of the adjacency effect on ground measurements. MODTRAN takes into account all four radiation components sketched in Fig. 1. In addition to ground geometry situations, the height dependence is computed for comparison to assess the relative importance of atmospheric backscattering and volume

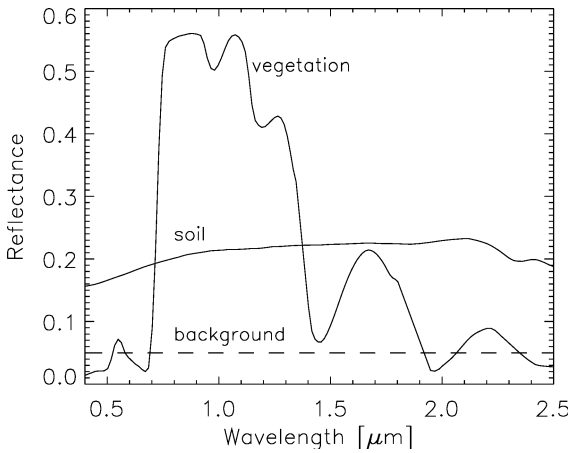

Fig. 7. Spectra of vegetation, soil, and background used for simulation.

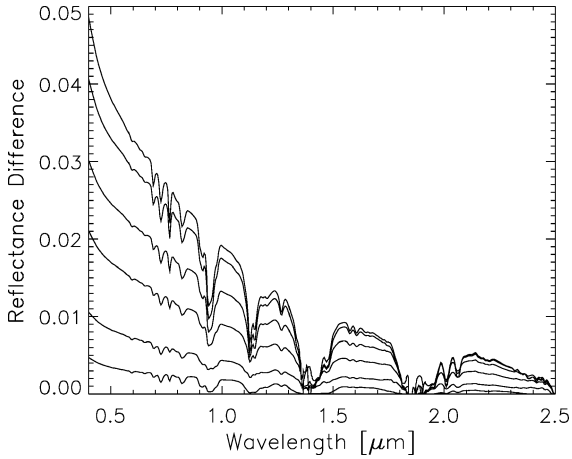

Fig. 8. Calculated spectral reflectance difference caused by the adjacency effect. Input are the soil/background spectra of Fig. 7. (Top to bottom curves) Sensor at 100, 5, 2, 1, and 0.3 km, and 1 m, respectively.

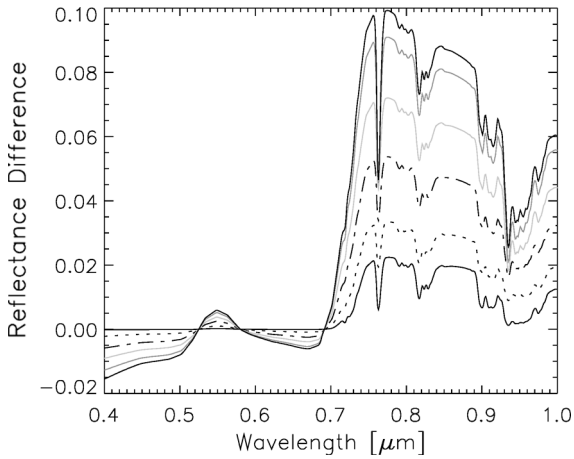

Fig. 9. Calculated spectral reflectance difference caused by the adjacency effect. Input are the vegetation/background spectra of Fig. 7. Top to bottom curves at 0.8 μm: sensor at 100, 5, 2, 1, and 0.3 km, and 1 m, respectively. The extracted zoomed spectral region is selected to focus on the situations with negative, zero, and maximum positive contrast.

scattering (components 3 and 4 of Fig. 1). We define two cases of practical interest (see Fig. 7).

1) A vegetation target in a dark tar background ($\rho_{\mathrm{b}} = 0.05$) with a large reflectance contrast of 0.5 units in the near-infrared (NIR) region. This contrast is also typical for water bodies and vegetation in the NIR.
2) A soil target in the same dark tar background with a reflectance contrast of 0.10 units in the blue part of the spectrum and a contrast of 0.17 in the 1.6-μm region.

MODTRAN calculations were performed for a large uniform vegetation and soil target, and for a single target pixel embedded in the large dark background. Typical clear sky conditions were used as simulation parameters: solar zenith angle 40°, a midlatitude summer atmosphere, rural aerosol, visibility 23 km, atmospheric water vapor column 2 cm, ground at sea level, and sensor 1 m above the ground. Results of MODTRAN are the total at-sensor radiance and path radiance (computed with ground reflectance $= 0$). To obtain results in terms of reflectance, the path radiance was subtracted from the total radiance, the radiance converted into the equivalent reflectance, and the difference $\Delta\rho$ of the target to the target/background situation was computed.

Fig. 8 presents an overview of the $\Delta\rho$ curves as a function of the sensor-target distance for the soil case. The maximum reflectance difference in the blue part of the spectrum is $\Delta\rho \approx 0.05$ units (100-km altitude) strongly decreasing with wavelength despite of an increase of the reflectance contrast. The difference is larger in the blue spectrum than for the vegetation/tar case (Fig. 9) because of the larger reflectance contrast. For the 1-m target-sensor distance $\Delta\rho \approx 0.005$ (at 0.4 μm), therefore, the volume scattering (radiation component 3) is about a factor of 9 greater at the 100-km range than the atmospheric backscattering contribution (component 4) in this scenario. In the 1.6-μm region the adjacency effect modifies the reflectance less than $\Delta\rho = 0.01$, and in the 2.2-μm region less than $\Delta\rho = 0.005$.

Fig. 9 summarizes the results for the vegetation case. Results are only shown for the zoomed spectral region 0.4–1 μm which contains the interesting situations with zero reflectance contrast and maximum contrast, i.e., no adjacency influence and maximum influence. The bottom curve (at 0.8 μm) corresponds to a 1-m distance, the top curve to a 100-km distance. The maximum reflectance difference (at 0.8 μm) is $\Delta\rho \approx 0.02$ units for the shortest distance; it increases with sensor height to $\Delta\rho \approx 0.10$ units for the 100-km range. The contrast becomes negative in the blue region where the reflectance of vegetation is smaller than that of the background. The plot shows that in the ground-based configuration only the atmospheric backscattering (radiation component 4) is relevant. With increasing measurement height the volume scattering (component 3) comes into play and actually represents the major contribution of the two adjacency components. For zero reflectance contrast situations (at 0.53 and 0.58 μm) the adjacency influence vanishes ($\Delta\rho = 0$). It can be stated that the influence of the atmospheric backscattering on ground measurements of small-area targets is difficult to measure because it requires a very high reflectance contrast and a very uniform target with an extremely low standard deviation of the reflectance.

IV. Conclusion

Ground reflectance measurements of two targets (garden cress and soil) were performed in two background types (concrete, dry meadow) to investigate the influence of the adjacency effect for short-range distances (< 2 m). In agreement with theoretical radiative transfer calculations, the influence of the adjacency effect was found to be very small for short-distance measurements. Nevertheless, these calculations also indicate critical configurations, e.g., for a reflectance contrast of 0.5 units in the NIR region, the atmospheric backscattering component of the adjacency effect accounts for a 0.02 reflectance unit change, which should be corrected when performing accurate field measurements of small-area targets. However, directional effects were not taken into account, and therefore it is not possible to draw a general conclusion, since some of the surfaces are known for exhibiting strong directional effects (e.g., garden cress). Of course, the adjacency effect is always important for long-range measurements from airborne and satellite sensors if the scene contains large reflectance contrasts.

References

[1] M. Jianwen, L. Xiaowen, C. Xue, and F. Chun, "Target adjacency effect estimation using ground spectrum measurement and Landsat-5 satellite data," *IEEE Trans. Geosci. Remote Sens.*, vol. 44, no. 3, pp. 729–735, Mar. 2006.

[2] W. A. Pearce, "A study of the effects of the atmosphere on Thematic Mapper observations," EG&G Washington Analytical Services Center, Inc., Riverdale, MD, Rep. 004-77, 1977.

[3] J. Otterman and R. S. Fraser, "Adjacency effects on imaging by surface reflection and atmospheric scattering: Cross radiance to zenith," *Appl. Opt.*, vol. 18, pp. 2852–2860, 1979.

[4] J. V. Dave, "Effect of atmospheric conditions on remote sensing of a surface nonhomogeneity," *Photogramm. Eng. Remote Sens.*, vol. 46, no. 9, pp. 1173–1180, 1980.

[5] Y. Meckler and Y. J. Kaufman, "The effect of Earth's atmosphere on contrast reduction for a nonuniform surface albedo and 'two-halves' field," *J. Geophys. Res.*, vol. 85, no. 20, pp. 4067–4083, Jul. 1980.

[6] D. Tanre, M. Herman, and P. Y. Deschamps, "Influence of the background contribution upon space measurements of ground reflectances," *Appl. Opt.*, vol. 20, no. 20, pp. 3676–3684, Oct. 1981.

[7] Y. J. Kaufman, "The atmospheric effect on the separability of field classes measured from satellites," *Remote Sens. Environ.*, vol. 18, no. 8, pp. 21–34, Aug. 1985.

[8] R. Richter, "A fast atmospheric correction algorithm applied to Landsat TM images," *Int. J. Remote Sens.*, vol. 11, no. 1, pp. 159–166, Jan. 1990.

[9] E. F. Vermote, D. Tanre, J. L. Deuze, M. Herman, and J. J. Morcrette, "Second simulation of the satellite signal in the solar spectrum, 6S: An overview," *IEEE Trans. Geosci. Remote Sens.*, vol. 35, no. 3, pp. 675–686, May 1997.

[10] P. N. Slater, S. F. Biggar, R. G. Holm, R. D. Jackson, Y. Mao, M. S. Moran, J. M. Palmer, and B. Yuan, "Reflectance and radiance-based methods for the in-flight absolute calibration of multispectral sensors," *Remote Sens. Environ.*, vol. 22, no. 1, pp. 11–37, Jun. 1987.

[11] R. Richter, "On the in-flight absolute calibration of high spatial resolution spaceborne sensors using small ground targets," *Int. J. Remote Sens.*, vol. 18, no. 13, pp. 2827–2833, Sep. 1997.

[12] R. O. Green, B. E. Pavri, and T. G. Chrien, "On-orbit radiometric and spectral calibration characteristics of EO-1 Hyperion derived with an underflight of AVIRIS and *in situ* measurements at Salar de Arizaro, Argentina," *IEEE Trans. Geosci. Remote Sens.*, vol. 41, no. 6, pp. 1194–1203, Jun. 2003.

[13] R. N. Clark, G. A. Swayze, K. E. Livo, R. F. Kokaly, T. V. V. King, J. B. Dalton, J. S. Vance, B. W. Rockwell, T. Hoefen, and R. R. McDougal, "Surface reflectance calibration of terrestrial imaging spectroscopy data: A tutorial using AVIRIS," in *Proc. 10th Airborne Earth Sci. Workshop*, 2002, pp. 43–63.

[14] *Analytical Spectral Devices*. [Online]. Available: http://www.asdi.com/products-spectroradiometers.asp

[15] J. V. Martonchik, D. J. Diner, B. Pinty, M. M. Verstraete, R. B. Myneni, Y. Knyazikhin, and H. R. Gordon, "Determination of land and ocean reflective, radiative, and biophysical properties using multiangle imaging," *IEEE Trans. Geosci. Remote Sens.*, vol. 36, no. 4, pp. 1266–1281, Jul. 1998.

[16] A. Berk, G. P. Anderson, P. K. Acharya, M. L. Hoke, J. H. Chetwynd, L. S. Bernstein, E. P. Shettle, M. W. Matthew, and S. M. Adler-Golden, *MODTRAN4 Version 3 Revision 1 User's Manual*. Hanscom Air Force Base, MA: Air Force Res. Lab., 2003.